

CONF-960569--9

The submitted manuscript has been authored by a contractor of the U. S. Government under contract DE-AC05-96OR24464. Accordingly, the U. S. Government retains a non-exclusive, royalty free license to publish or reproduce the published form of this contribution, or allow others to do so, for U. S. Government purposes.

RECEIVED  
SEP 19 1996  
OSTI

## Plasma-surface interactions with ICRF antennas and lower hybrid grills in Tore Supra

J. H. Harris<sup>1</sup>, T. Hutter<sup>2</sup>, J. T. Hogan<sup>1</sup>, V. Basiuk<sup>2</sup>, B. Beaumont<sup>2</sup>, A. Becoulet<sup>2</sup>,  
S. Bremond<sup>2</sup>, M. D. Carter<sup>1</sup>, M. Goniche<sup>2</sup>, R. H. Goulding<sup>1</sup>, D. Guilhem<sup>2</sup>,  
G. R. Haste<sup>1</sup>, D. J. Hoffman<sup>1</sup>, H. Kuus, L. Ladurelle<sup>2</sup>, X. Litaudon<sup>2</sup>,  
F. Nguyen<sup>2</sup>

<sup>1</sup>*Oak Ridge National Laboratory, Oak Ridge, Tennessee, USA*

<sup>2</sup>*Centre d'Etudes de Cadarache, Association EURATOM-CEA sur la Fusion,  
St. Paul lez Durance, France*

presented at the

MASTER

12th International Conference on  
Plasma-Surface Interactions in Controlled Fusion Devices

St. Raphael, France

May 20-24, 1996

DISTRIBUTION OF THIS DOCUMENT IS UNLIMITED

#### **DISCLAIMER**

**Portions of this document may be illegible  
in electronic image products. Images are  
produced from the best available original  
document.**

## **DISCLAIMER**

This report was prepared as an account of work sponsored by an agency of the United States Government. Neither the United States Government nor any agency thereof, nor any of their employees, makes any warranty, express or implied, or assumes any legal liability or responsibility for the accuracy, completeness, or usefulness of any information, apparatus, product, or process disclosed, or represents that its use would not infringe privately owned rights. Reference herein to any specific commercial product, process, or service by trade name, trademark, manufacturer, or otherwise does not necessarily constitute or imply its endorsement, recommendation, or favoring by the United States Government or any agency thereof. The views and opinions of authors expressed herein do not necessarily state or reflect those of the United States Government or any agency thereof.

# Plasma-surface interactions with ICRF antennas and lower hybrid grills in Tore Supra

J. H. Harris<sup>1</sup>, T. Hutter<sup>2</sup>, J. T. Hogan<sup>1</sup>, V. Basiuk<sup>2</sup>, B. Beaumont<sup>2</sup>, A. Becoulet<sup>2</sup>,  
S. Bremond<sup>2</sup>, M. D. Carter<sup>1</sup>, M. Goniche<sup>2</sup>, R. H. Goulding<sup>1</sup>, D. Guilhem<sup>2</sup>, G. R. Haste<sup>1</sup>,  
D. J. Hoffman<sup>1</sup>, X. Litaudon<sup>2</sup>, F. Nguyen<sup>2</sup>

<sup>1</sup>*Oak Ridge National Laboratory, Oak Ridge, Tennessee, USA*

<sup>2</sup>*Centre d'Etudes de Cadarache, Association EURATOM-CEA sur la Fusion,  
St. Paul lez Durance, France*

**Abstract.** The edge plasma interactions of the actively cooled radio-frequency heating launchers in Tore Supra—ion-cyclotron range-of-frequencies (ICRF) antennas and lower-hybrid (LH) grills—are studied using infrared video imaging. On the two-strap ICRF antennas, operated in fast-wave electron heating or current drive mode, hot spots with temperatures of 500–900° C are observed by the end of 2-s power pulses of 2 MW per antenna. The distribution and maximum values of temperature are determined principally by the relative phase of the two antenna straps: dipole (heating) phasing results in significantly less antenna heating than does 90° (current drive) phasing. Transient heat fluxes of 1–20 MW/m<sup>2</sup> are measured on the lateral protection bumpers at ICRF turn-on; these fluxes are primarily a function of plasma and radio frequency (rf) control, and are not simply correlated with the strap phasing or the final surface temperature distributions. The remarkable feature of the lower hybrid edge interaction is the production of beams of heat flux in front of the grills; these beams propagate along the helical magnetic field lines and can deliver fluxes of 5–10 MW/m<sup>2</sup> over areas of several cm<sup>2</sup> to plasma-facing components such as the grill or antenna lateral bumpers. Both the ICRF and LH phenomena appear to result from the acceleration of particles by the near fields of the launchers. Modeling of the heat flux deposition on components and its relation to sputtering processes is presented, and possibilities for controlling these interactions are discussed.

## 1. Introduction

The goal of present experiments [1] on the Tore Supra tokamak is to sustain advanced tokamak operation under near steady-state conditions using rf heating. Two rf systems are used: an ICRF system which delivers 5–10 MW through three two-strap antennas, and a LH system which delivers 4–6 MW through two wave guide array couplers. The ICRF system is presently run principally in a fast-wave electron heating (FWEH) mode, which produces high bootstrap current fractions; the two current straps in each antenna can also be phased for fast-wave current drive (FWCD). The LH system is used for long pulse current drive. While both systems are capable of delivering power in steady-state, plasma heating operation is in practice limited by heating of launcher components (most importantly the carbon tiles on the lateral protection bumpers) to

temperatures of  $\geq 1000^{\circ}\text{C}$ . Once tiles are damaged, the effectiveness of the active cooling is reduced, and it is necessary to limit the pulse length to avoid excessive temperature rise.

Earlier video imaging studies [2] of visible carbon and infrared (IR) emission from the antennas and grills show some qualitatively similar features. Diffuse carbon III (CIII) emission from the antenna or grill regions rises within  $\sim 50$  ms of the application of either ICRF or LH power, while IR hot spots appear on longer time scales 0.2–1.0 sec. The CIII emission from the LH grills shows transient striations aligned along the wave guide mouths, while the CII emission from the LH grills also shows localized emission bursts that appear to originate in the wave guide mouths. The predominance of the CIII emission may be evidence of impurity migration to the antenna grill regions from elsewhere in the torus.

In sections 2 and 3 of this paper, we describe detailed IR video imaging studies of edge interactions involving ICRF antennas and LH launchers. We show temperature distributions and their evolution and heat fluxes on rf components, and relate these phenomena to the rf fields imposed by the launcher structures. In section 4, we present the results of a modeling study of the LH launcher edge interaction that incorporates plasma and surface physics effects. In section 5, we discuss conclusions and possible remedies to improve the performance of rf edge components.

## 2. ICRH antenna interaction experiments

A controlled set of experiments was done to acquire thermal imaging data on an as-yet undamaged ICRF antenna under Tore Supra operating conditions used for advanced tokamak experiments. Two antennas were energized simultaneously: an antenna already in service for some time in port Q1 and a new antenna developed at Oak Ridge National Laboratory (ORNL) and being tested for the first time in port Q5. The new antenna is intended to improve coupling and features a reduced spacing between the current straps and the Faraday screen, a slightly longer effective current strap length, and a recessed septum to improve the coupling spectrum for current drive and to improve thermal performance. Both antennas have carbon tile bumpers and Faraday screens coated with B<sub>4</sub>C.

The discharge parameters were  $B_T = 2.15$  T,  $I_p = 0.68$  MA,  $q_\psi \approx 4.6$ , and  $\langle n_e \rangle \approx 3 \times 10^{19}$  m<sup>-3</sup>. The antennas were energized simultaneously for 2.5 s at  $f = 48$  MHz (fast wave electron heating/current drive mode), and  $P_{\text{rf}} = 2$  MW for each antenna. Figure 1 shows the discharge traces for two shots in a sequence. In shot 19708, both antennas were energized with their current straps phased 180° (dipole mode) for FWEH, and in shot 19710, the Q5 antenna had its straps phased to 90° for FWCD (co-current drive). In both shots, the antenna-plasma distance dropped

from 3-4 cm to 1-2 cm as the rf power rose. The general behavior of the discharge traces for the two shots is similar, although for shot 19710 (Q5 phased for FWCD) there are several dropouts of the ICRF on the Q5 antenna before coupling is established.

The analysis of antenna surface heating presented here focuses on the new ORNL antenna in Q5, because its lateral protection bumpers were still smooth and undamaged, so that the effects of rf power could be separated from those of surface imperfection, projections, etc. Figure 2 compares IR images and time histories of selected zones on the antenna (4 pixels averaged, resolution ~2 cm) for dipole and FWCD operation of the antenna. The IR images were taken just before rf turn-off at  $t \approx 6.5$  s, and the framing rate of the camera was 50 frames a second, so the time resolution of the temperature traces is 0.02 s.

The surface heating patterns for dipole and FWCD phasing show substantial qualitative and quantitative differences. In dipole mode, the regions of strongest surface heating are the two lateral bumpers, with the hottest regions falling near the equatorial midplane (points *a* and *c* on the dipole image in Fig. 2). (There is also a region of some heating on the lower edge of the antenna box; this was found to be due to a protrusion of one edge of the antenna box, which has been subsequently cut back). The temperature rises rapidly (~0.2 s) and then decreases somewhat before becoming approximately constant. This may be evidence of a local reduction in heat flux, as the thermal time scale for active cooling of the bumper is 1-2 seconds, much longer than the time scale over which the decline in temperature occurs.

In contrast, for FWCD phasing, not only the bumpers but the entire midplane region of the antenna heats up. Additional hot spots are seen on the lower corners of the antenna (points *d* and *f* in Fig. 2). Many of the hot zones continue to increase in temperature throughout the rf pulse. Note that the septum located at the midline of the antenna does not heat because the tubes of the Faraday screen bend away from the plasma by about 2 cm there.

Shots were also taken with the Q5 antenna straps phased at 270°, i.e., for counter-current drive. The surface heating pattern is essentially the same as that for 90° phase. An interesting detail is that the location of the hottest of the lower corner points changes sides, i.e., moves from point *f* to point *d* in Fig. 2, when the strap phase is changed from 90° to 270°.

The Q1 antenna shows surface heating patterns qualitatively similar to those seen on the Q5 antenna. The maximum temperatures on the bumpers were higher (800° for dipole operation), but many of the hot tiles showed signs of previous damage—they remained hot for seconds after the rf power turn-off, indicating that their contact with the cooled bumper structure had been damaged—so these data are difficult to interpret in detail.

Studies of the temperature history during the initial rise in surface temperature showed that it fit a  $t^{1/2}$  curve, as expected for a solid heating on its inertial time scale. The temperature data could thus be used to calculate an equivalent normal heat flux based on the model of the semi-infinite solid [3]. The heat flux on the contour shown on the right-side bumper of the Q5 antenna during the fast temperature rises in shots 19708 and 19710 is shown in Fig. 3. The calculated fluxes in this case are quite large, with peak values  $\sim 15\text{--}20 \text{ MW/m}^2$ , peaked on the equatorial midplane. These fluxes occur for only  $\sim 0.2\text{--}0.3 \text{ s}$ , after which the temperature rise slows or even ceases (Fig. 2). Studies of other shots with different plasma control details show significantly different fluxes. For example, for another dipole/FWCD comparison (shots 19700 and 19701), the plasma was moved to  $\sim 2 \text{ cm}$  from the antennas, and the rf power was raised slowly to 2 MW over 1.5 s. In this case, the initial temperature rise is much slower ( $\approx 1 \text{ s}$ ) and the calculated fluxes along the right lateral bumper have maxima of 1 MW (dipole) and 3 MW (FWCD). Nevertheless, the final surface temperature distributions at the end of the rf pulse are essentially the same as for the respective cases shown in Fig. 2. This suggests that while operational details may affect the transient heat flux that falls on the antenna at rf power-on, the final (steady state) heating pattern is primarily determined by the geometric structure of the rf field in front of the antenna.

Laboratory measurements with a directional detector of the poloidal rf electric field—the principal drive launched by the current strap—in front of the unloaded antenna (Fig. 4) show the essential difference between dipole and FWCD operation. The dipole configuration has a field null on the antenna septum where the field changes sign, while the FWCD configuration has only a slight dip. Vertical scans of the poloidal component show that it has a broad maximum on the equatorial midplane. Measurements of the radial component (normal to the antenna face) show substantially higher maxima at the top and bottom of the antenna for FWCD phasing. Detailed modeling of the field structure in the presence of plasma loading is being carried out using a modified version of the RANT-3D code [4].

Taken as a whole, these results suggest that the pattern of antenna surface heating is closely related to the rf field directly in front of the antenna, and presumably the resultant particle acceleration and charge flows. Dipole phasing reduces the antenna heating by reducing the rf field near the antenna. It is tempting to apply a sheath rectification analogy [5]. If we use effective potential values of 1-10 kilovolts, comparable to the rf potentials in front of the antenna, the equivalent current densities required to produce power fluxes like those measured at power turn on are  $100\text{--}1000 \text{ A/m}^2$ .

### 3. LH coupler interaction experiments

Previous studies [2] of the interactions of the LH couplers with the edge plasma showed that beams of heat flux emanate along the centerline of each wave guide row and impinge upon the bumpers on both sides of the grill, leading to significant temperature rises of 400°C or more. Calculations of local electron acceleration directly in front of the grill showed that the electron distribution function broadens, with tail energies in the range of 3–5 keV and mean electron energies of 300–500 eV. Such populations can be expected to lead to the heating observed on the lateral bumpers of the LH launcher, and section 4 describes a model of the interaction of the accelerated electrons with the bumper surfaces.

Recent experiments have shown that the beams of heat flux pass beyond the bumpers and follow the magnetic field lines, where they can strike other plasma-facing components. By adjusting the plasma current [and hence the edge safety factor  $q(a)$ ] it is possible to place the beams on particular components whose response can be monitored using the IR imaging system. By choosing  $q(a)$  so that the LH couplers are magnetically connected to a vertical limiter, and then varying  $q(a)$  slightly and firing the two couplers in succession, it has been possible to identify the hot spots that result from each of the four rows of wave guides in the two couplers. The total power carried in these beams is small,  $\leq 1\%$  of the LH power launched by the couplers, but locally elevated fluxes can cause damage to plasma facing components.

A dramatic example of the effect of these LH produced heat fluxes on another component—an ICRF antenna—is illustrated in Fig. 5. In this case, magnetic field lines connect the grill with the lateral bumper of the antenna. The resulting heat flux on the bumper produces hot spots and damages bumper tiles. Use of the heat flux estimation technique described in section 2 produces the profile of heat flux along the bumper shown in Fig. 5. The peak values of  $\sim 8 \text{ MW/m}^2$  shown reflect an average over zones of size  $\sim 1 \text{ cm}$ . If the plasma beams are in fact smaller, the local flux values would be higher.

### 4. Modeling of the LH surface interaction

An evaluation of the mechanisms involved in the interaction of the LH-accelerated electrons with the lateral bumpers on the grill or the ICRF antenna has been carried out using the BBQ impurity SOL transport code and the CASTEM-2000 finite element thermal analysis code. The input SOL parameters for modeling are based on reciprocating Langmuir probe profiles for similar discharges. Because the incident heat flux to the surface of the lateral protection depends on the instantaneous temperature of the surface, and this surface is actively cooled, a self-consistent

thermal analysis is required, including the instantaneous local sheath potential. Fast electron, thermionic emission, and secondary electron emission effects on the sheath potential have thus been included in CASTEM. The heat flux conducted away from the wall is calculated by CASTEM, and includes contributions due to bulk conduction, thermal radiation, evaporative and thermionic cooling. The model calculates the condition of zero net electron current to the surface:

$$n_e v_e e e^{-e\Phi/T} \beta / 4 - J_T = \Gamma_i e$$

where

$$v_e = (8 T_e / \pi m_e)^{1/2},$$

$$\Gamma_i = n_i V_s$$

$$V_s = [(T_i + T_e) / m_i]^{1/2}$$

$$\beta = (1 - \sigma_{se}) / (1 + \sigma_{si}),$$

$\sigma_{se,i}$  are the secondary electron and ion emission coefficients, and  $J_T$  is the thermionic current. Thus, the heat flux from the plasma to the wall is:

$$q_{ps} = \gamma \Gamma_i T$$

where

$$\gamma = 1 + \Phi + z_T$$

$$\Phi = e\phi/T = \ln [(m_i / \pi m_e)^{1/2} / z_T]$$

$$z_T = 2 (1 + y_T) / \beta,$$

$$y_T = J_T / e\Gamma_i.$$

The heat flux enhancement due to a fast-electron minority with average energy  $\sim 10$  times greater than the bulk is included, using the model described in Ref. 6. This calculation predicts a substantial increase in the heat flux transmitted through the sheath, due to a decrease in  $\Phi$ . This reduction in potential allows direct fast electron heating. For the conditions estimated for the Tore Supra LH couplers, the fast electron population is  $\sim 10\%$  of the bulk population, with a mean energy  $\sim 10$  times the background  $T_e$ .

The analysis of the allowable operating regime consists of evaluating the particle balance for two species ("high" and "low" energy) of C impurities, as described in Ref. 7. Physical sputtering produces a Thomson distribution of particles with higher energies ( $>1$  eV), whereas processes such as chemical sputtering and radiation-enhanced sublimation (RES) produce thermal particles with lower energy ( $E_L \sim 0.1$  eV). The latter are more likely to be ionized close to the surface (within the magnetic Debye sheath) and redeposited on the surface without being accelerated by the sheath, while the former may be redeposited at the surface with a high energy ( $E_H = \gamma kT_e$ , with  $\gamma \sim 3$ ). The total flux of C atoms with "high" energy ( $\Gamma_H^T$ ) is thus the sum of fluxes of the original, physically sputtered particles [with yield  $Y_{D+}^{\text{Phys}}$  ( $E_{sh}$ )] and of the flux of particles produced by sputtering due to the redeposited fluxes (with redeposition coefficients  $R_H$  and  $R_L$ ) which strike the surface with  $E_H$  and  $E_L$ , respectively.

Additional terms have been added in to those in the original analysis [7] to include low-energy chemical sputtering self-consistently and to include the low energy particles produced by evaporation at very high temperatures, where thermionic emission effects are important. The revised low-energy particle balance thus introduces chemical, RES, and thermionic effects. The basic data used in this model are the physical, chemical, and RES sputtering yields, updated [8] to account for the "athermal" mechanism which produces chemical sputtering at lower temperatures than have been previously considered. The impurity runaway condition determines the limit to the predicted allowable operating space. The analysis has been updated by including: (1) the localized redeposited heat flux due to C impurities and increased physical sputtering coefficients for D incident on C; (2) the dependence of the incident heat flux on the secondary electron emission (SEE) coefficient ( $\sigma_{se}$ ); and (3), including the effects of the LH fast electrons on the sheath potential. The resulting operational space for cases with  $n_{\text{hot}}/n_{\text{bulk}}=2\%$  and  $T_{\text{hot}}/T_{\text{bulk}}=1$  to 1000, is shown in Fig. 6.

The operational space with inclusion of fast electron effects may be limited to  $T_e(\text{SOL}) < 60$  eV and  $1500 < T_{\text{surf}} < 2500$  K. The Tore Supra LH lateral protection is actively cooled, so that under normal conditions, such a high surface temperature would not be attained. However, localized overheating is still possible, and the production of strongly localized heat fluxes due to redeposition of impurities and fast electron sheath effects could produce the observed local CII and  $H_{\alpha}$  hot spots. CASTEM was used to examine local impurity production and it was found that sharply localized chemical production can occur as T approaches 1000°K. Thus, a strongly local source of CII and  $H_{\alpha}$  could appear at temperatures that are observed in the experiments.

## 5. Discussion

These studies show that the launching of rf power into the tokamak edge plasma can result in substantial heat fluxes to the rf launchers themselves and to other components connected to them by the helical magnetic field lines. These fluxes pose practical difficulties for the maintenance of steady-state plasmas.

Some reduction of the fluxes can be effected by optimizing the rf field configuration of the launcher so as to minimize stray rf components, as is shown with dipole phasing of the ICRF antenna straps. Antenna design changes to improve coupling (as with the new ORNL antenna on Tore Supra) may also help reduce particle acceleration in the plasma edge. Measurements of the energy and type of particles that carry the heat flux would be valuable in improving models for the particle acceleration process in front of the launchers.

Mitigation of the effects of the fluxes on other components involves control of the magnetic connections of the launchers. Sweeping of the radial position of the launcher or a small time-variation of  $q(a)$  may be effective ways of reducing the peak values of heat flux to connected components, and experiments to address this are being planned for Tore Supra. Improved bumper designs (larger sloping surfaces, more efficient cooling) and material coatings (e.g., B<sub>4</sub>C) that reduce impurity production can improve the response of components to the high fluxes; efforts in these areas are also underway for Tore Supra.

This work was supported in part by the Office of Fusion Energy, U.S. Department of Energy, under contract DE-AC05-96OR22464 with Lockheed-Martin Energy Research Corporation.

## References

1. Equipe Tore Supra, *Plasma Phys. Contr. Nucl. Fusion* **36**, B123 (1994).
2. J. H. Harris *et al*, *Proc. 22nd European Physical Society Conference on Controlled Fusion and Plasma Physics*, Part IV, p. 397 (1995).
3. H. S. Carslaw and J. C. Jaeger, *Conduction of Heat in Solids*, Oxford University Press, 1984.
4. M. D. Carter *et al*, *Nucl. Fusion* **36**, 209 (1996).
5. J-M Noterdaeme and G. Van Oost, *Plasma Phys. Contr. Nucl. Fusion* **35**, 1481 (1993).
6. K. Sato and F. Iwasaki, *Natl. Inst. of Fusion Science Rept. NIFS-136* (1992).
7. J. N. Brooks, *J. Nucl. Mat.* **170**, 164 (1990).
8. C. Garcia-Rosales and J. Roth, *Proc. 21nd European Physical Society Conference on Controlled Fusion and Plasma Physics*, Part II, p. 397 (1994).

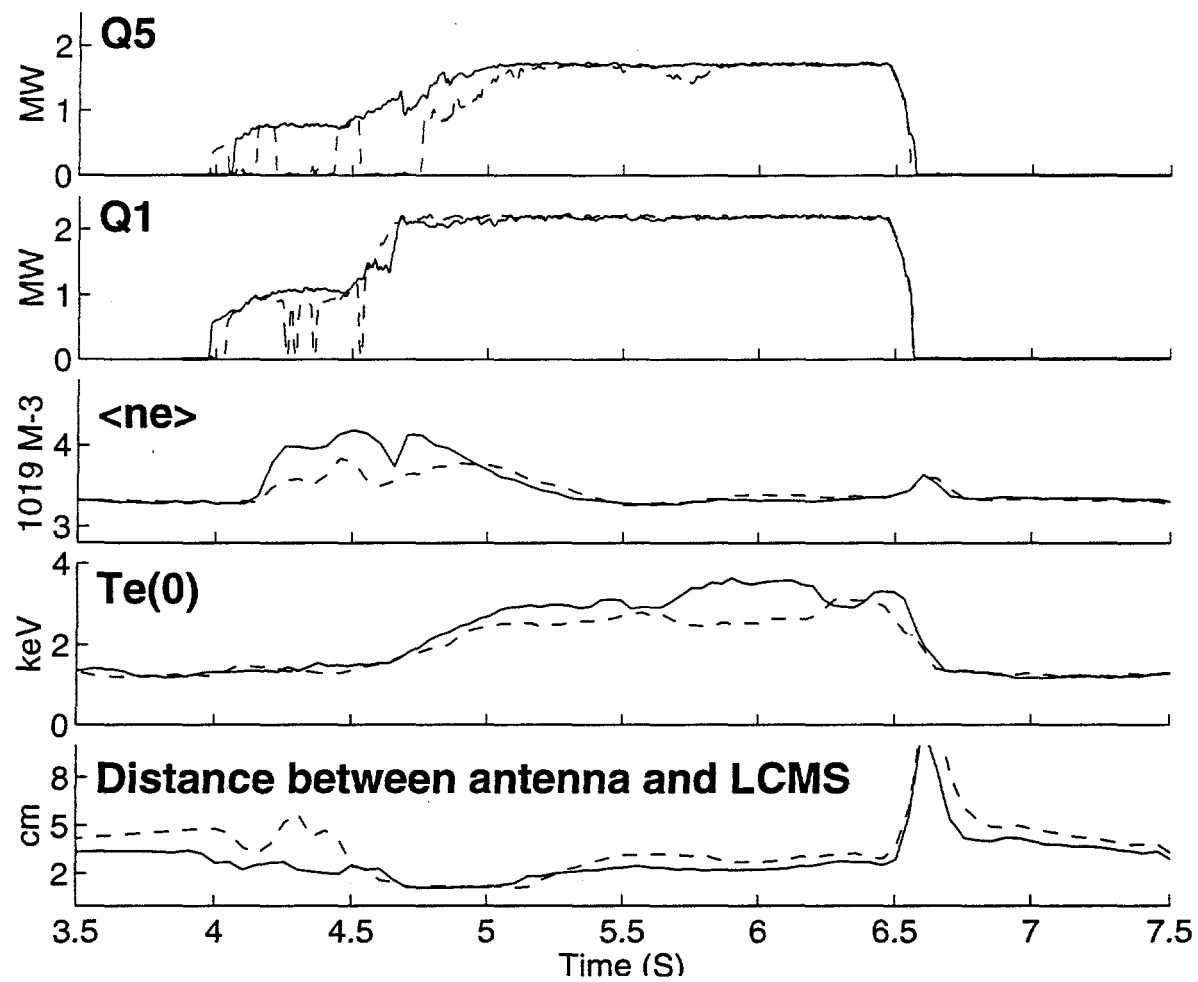
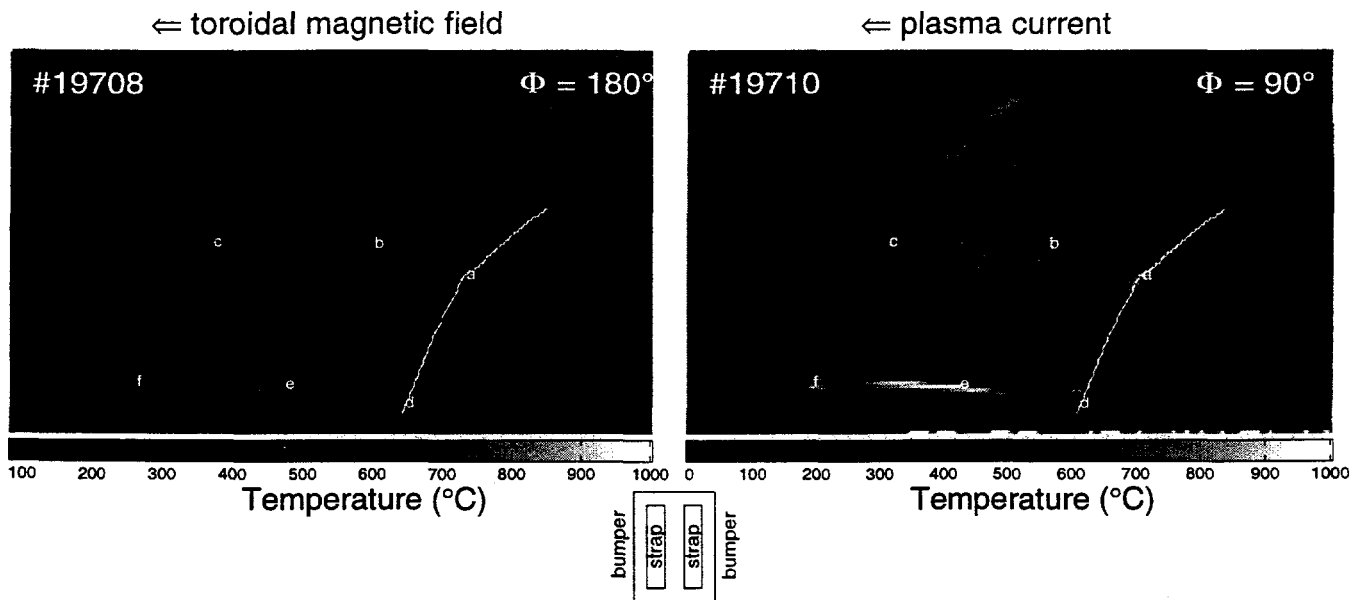


Fig 1. Diagnostic signals for Tore Supra ICRF heating shots. The solid lines show the signals for shot 19708, for which both the Q1 and Q5 antenna straps were phased at  $180^\circ$  (dipole, FWEH), and the dotted lines show the signals for shot 19710, for which the Q5 antenna straps were phased  $90^\circ$  (FWCD) while the Q1 antenna remained phased at  $180^\circ$ . The top two sets of traces, labeled Q1 and Q5, show the power launched by the respective antennas. The bottommost signals show the distance from the antenna to the last closed magnetic surface (LCMS).



Temperature histories ( $^\circ\text{C}$ ) at points labeled in IR images

— shot 19708 (Q5 dipole)      - - - - shot 19710 (Q5 FWCD)

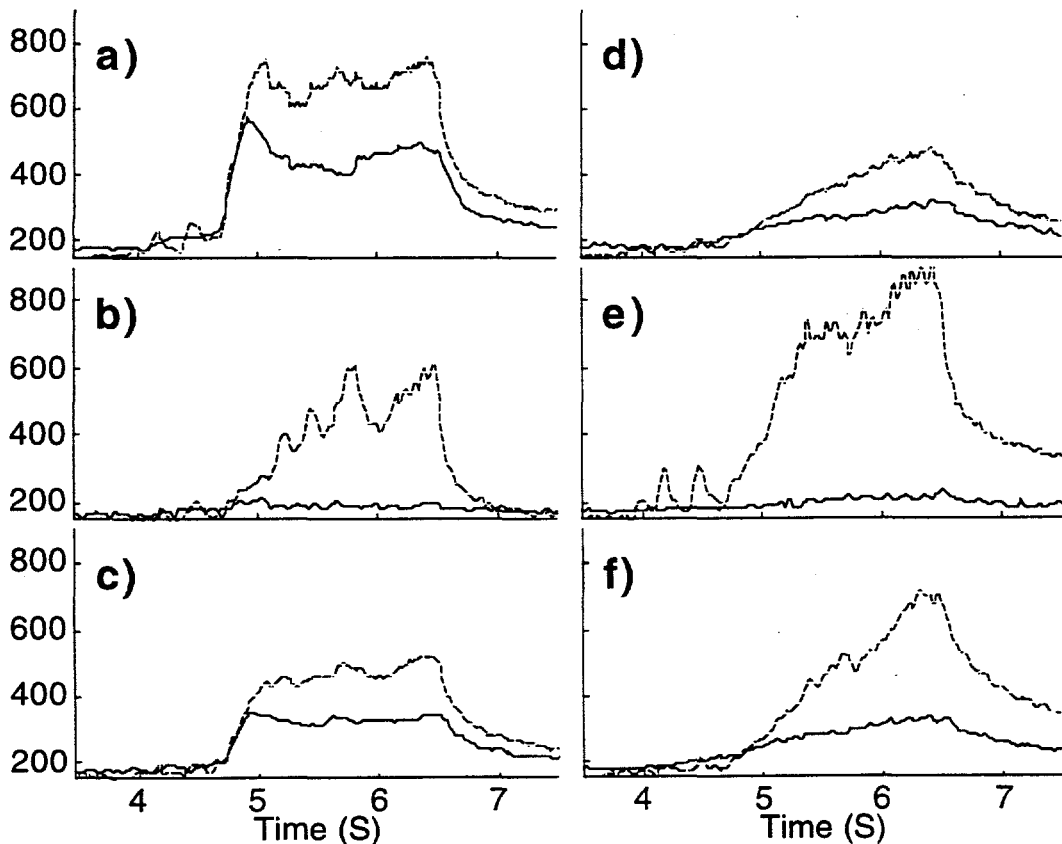


Fig. 2. Infrared images of Q5 (ORNL) antenna for both dipole and FWCD co-current drive strap phasing at end of heating pulse, together with time histories of temperatures for the labeled points in the images. The inset shows a schematic of the antenna, whose image is tilted by the IR optical system. The white lines on the right-hand side bumpers in the IR images indicate the contours for the heat flux profiles shown in Fig. 3.

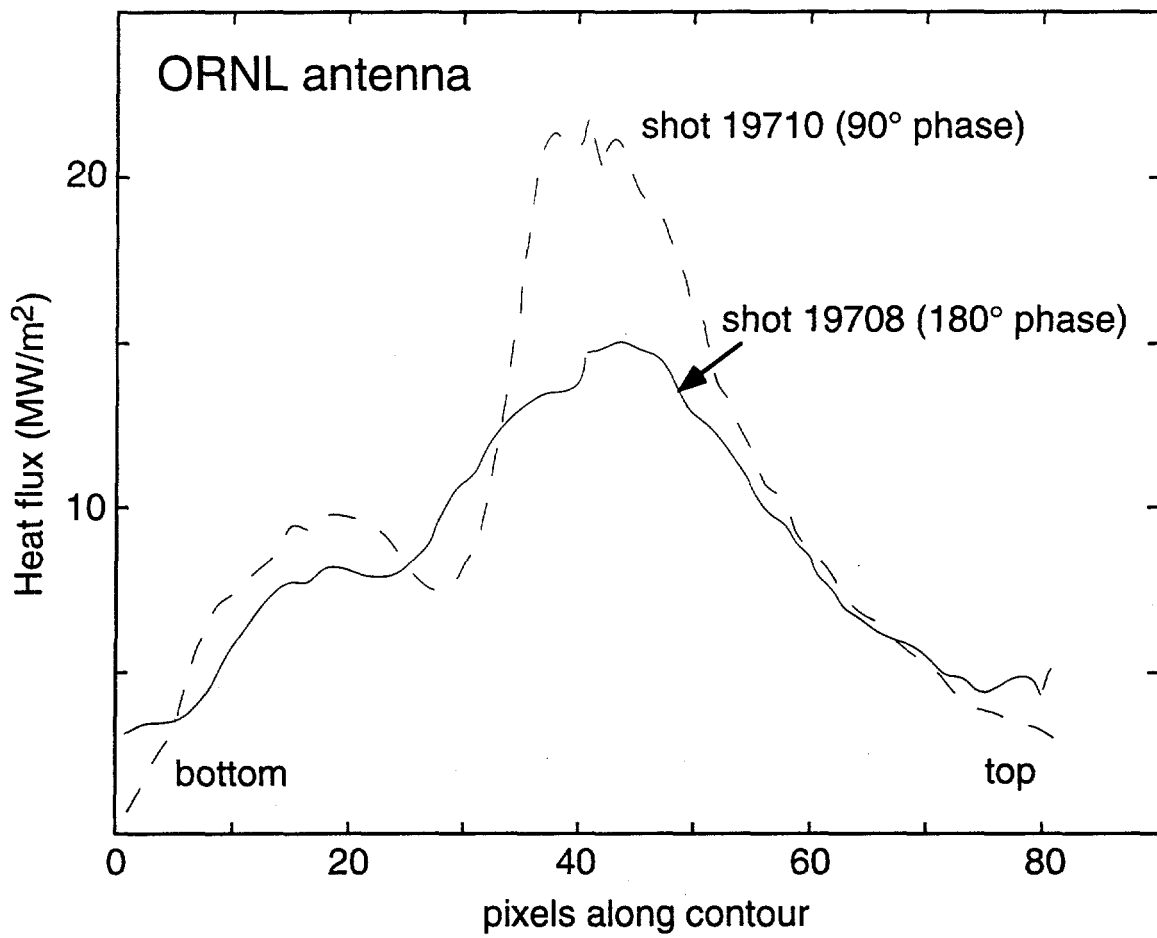


Fig. 3. Heat flux profile on lateral protection bumper contours shown in Fig. 2. Measurements made during period of fast surface temperature rise, 4.7–5.0 s.

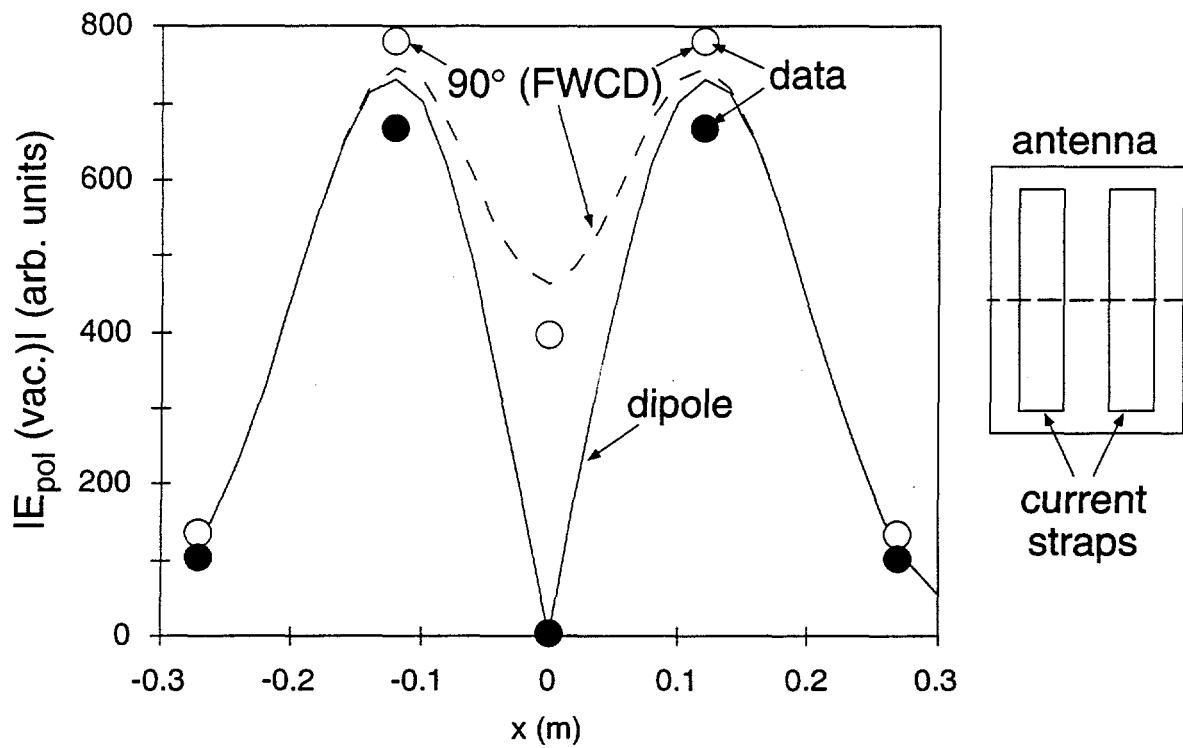


Fig. 4. Rf poloidal electric field measured 1 cm in front of Faraday screen of ORNL antenna. In the dipole configuration, there is a null in the field magnitude on the center line.

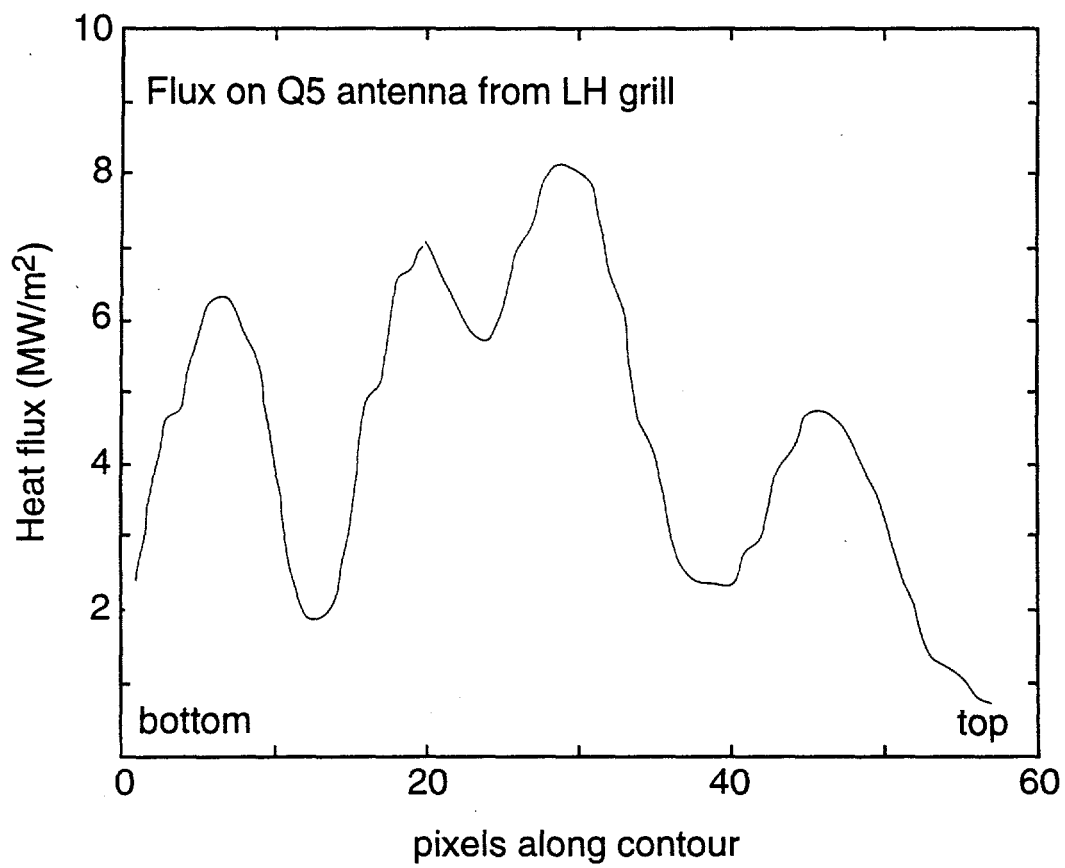
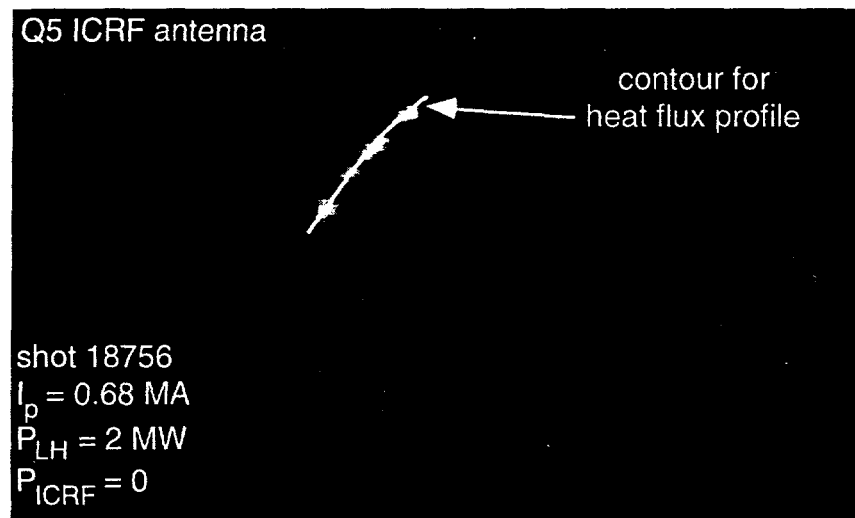


Fig. 5. Infrared image of unpowered ICRF antenna during LH heating, with LH grill magnetically connected to ICRF lateral protection limiters, together with measured heat flux profile along the contour shown. The hot spots reach 800° C in approximately 1 sec.

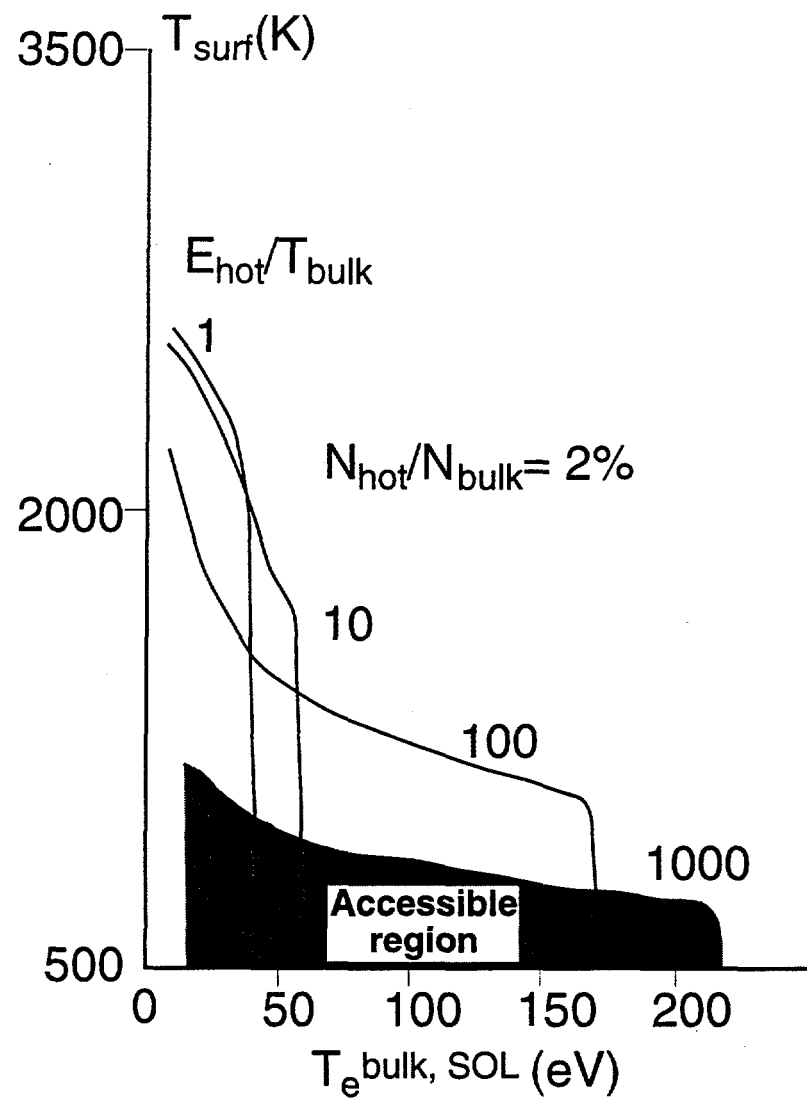


Fig. 6. Operating space for carbon plasma facing component (e.g., lateral protection bumper of LH coupler) subjected to fast electron as well as thermal plasma fluxes.